SUPPORTING INFORMATION

Design and synthesis of a heteroatom-rich Ni-MOF with a rare bis(μ-aqua) core for polarity-mediated heterogeneous catalysis

Sumedha Rana, Gouri Chakraborty and Sanjay K. Mandal*

Department of Chemical Sciences, Indian Institute of Science Education and Research Mohali, Mohali, Punjab 140306, India

*Author for correspondence:

Prof. Sanjay K. Mandal

E-mail: sanjaymandal@iisermohali.ac.in

TABLE OF CONTENTS

SECTION S1

Materials and Physical Measurements

All the chemicals and solvents used in the synthesis and subsequent studies were purchased from commercial sources and employed without further purification.

A comprehensive set of characterization techniques, including FTIR spectroscopy, Thermogravimetric analysis (TGA), X-ray diffractometry, Field emission scanning electron microscopy (FESEM), and X-ray photoelectron spectroscopy (XPS), was employed to thoroughly investigate the structural, morphological, and compositional features of the material. The Fourier-transform infrared (FTIR) spectra were obtained using a Shimadzu spectrometer. The samples were finely ground with KBr to form transparent pellets, and the spectra were recorded in the wavelength range of 4000-500 cm^{-1}. NMR spectra were recorded on a Bruker Biospin Avance-III spectrometer operating at 400 MHz. Microscopic analysis was performed by sonicating the sample in hexane, drop-casting the suspension onto carbon tape and a copper grid, and drying it under vacuum for 30 minutes. XPS analysis was performed using a K-α Plus XPS system under ultra-high vacuum ($\sim 10^{-9}$ torr) with Al Kα radiation.

The microscopic images for Field Emission Scanning Electron Microscopy (FESEM) analysis of **Ni-MOF** were taken in JEOL instrument using a working distance of 4.5-15 mm and a voltage of 5-15 kV. For the sample preparation, the methanolic suspension was prepared by sonication for 2-3 minutes and drop-casted on a silicon wafer. The sample was dried for 30 minutes in vacuum, and coated with gold. The energy dispersive X-ray spectroscopy (EDX) for mapping of elements was also carried out with the same instrument.

TGA was carried on a Shimadzu DTG-60H analyzer using aluminum pans with samples heated from 30 to 500 °C at 10 °C min^{-1} under nitrogen flow. Elemental analysis (C, H, and N) was carried out using a Thermo Finnigan analyzer.

Powder X-ray diffraction measurements were performed on a Rigaku Ultima IV diffractometer equipped with a 3 kW sealed-tube Mo Kα radiation source (λ = 0.71073 Å; generator settings: 40 kV, 40 mA) and a DTex Ultra detector. Data were collected in parallel beam geometry using 2.5° primary and secondary solar slits, a 0.5° divergence slit, and a 10 mm height limit slit. The samples were prepared as fine powders, placed in a glass sample holder, and positioned on a rotating stage attachment.

Single-crystal X-ray diffraction data were collected on suitable Ni-MOF crystals mounted on a nylon loop with Paratone-N oil. Measurements were performed at 100 K using a Kappa APEX II diffractometer equipped with sealed-tube MoKα radiation, a monochromator, and a CCD detector (50 mm crystal-to-detector distance). Unit-cell determination, data integration, reflection profile fitting, and calculation of F^2 and $\sigma(F^2)$ were carried out using SAINT, followed by Lorentz and polarization corrections. The data collection was done at 100 K. The crystal centering, unit cell determination, refinement of the cell parameters and data collection was monitored through APEX3 program.[S1] Space-group assignment, absorption correction (SADABS)[S1], data merging, and preparation of refinement files were performed via XPREP. The structure was solved with SHELXS and refined with SHELXL in Olex2.[S2] All non-hydrogen atoms were refined anisotropically. All figures were drawn using Mercury v3.10.2.S4, OLEX2, Viewer Lite and TOPOS Pro software.[S3,S4] Final refined coordinates and thermal parameters are provided in the respective CIF files.

Gas adsorption measurements were performed using a BELSORP MAX instrument at varying temperatures. Prior to the gas sorption experiments, samples degassing was done for 16 h at 120 °C under vacuum which was maintained by oil-free vacuum pump. Ultra-high-purity carrier gases (99.999% zero air and He) and oil-free pressure regulators were employed to prevent contamination during the measurement.

The ICP-MS studies were carried out with an Agilent 7850 instrument. The sample for measurement was prepared by filtering the reaction mixture three times, taking a 0.5 mL aliquot and diluting it with 4.5 mL of 10% HNO_3.

The theoretical structure of the **Ni-MOF** was optimized using DMol³ and Forcite simulations in BIOVIA Materials Studio 21.1.[S5] QTAIM analysis was conducted using Density Functional Theory (DFT) calculations performed with the Gaussian 09 software package.[S6] The structure was optimized using B3LYP (for C,H,N,O), which is a hybrid Becke's three parameter exchange and the Lee Yang-Par Correlation functional, and LANL2DZ (for metals) functional. A split valence basis set 6-31G+(d,p) is used for the calculation. Multiwfn and VMD softwares were used to obtain the bond critical points of the model compounds.[S7,S8]

SECTION S2

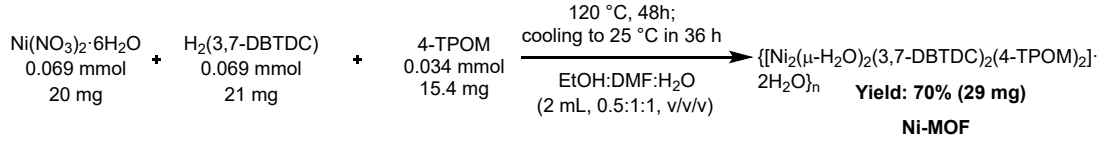

Scheme S1. Synthesis of Ni-MOF.

SECTION S3

Table S1. Crystallographic data and structure refinement parameters for **Ni-MOF**.

Compound	**Ni-MOF**
Chemical formula	$C_{78}H_{68}N_8Ni_2O_{24}S_2$
Formula weight (g mol^{-1})	1682.94
Temperature (K)	100.0(2)
Wavelength (Å)	0.71073
Crystal system	Triclinic
Space group	$P\bar{1}$
a (Å)	10.2167(11)
b (Å)	13.6751(15)
c (Å)	14.3129(16)
α (°)	90.8060(10)
β (°)	103.7530(10)
γ (°)	96.5960(10)
Z	1
V (Å^3)	1927.8(4)
Density (g cm^{-3})	1.450
μ (mm^{-1})	0.627
F (000)	872
θ (°) Range for data coll.	1.47 to 25.05
Reflections collected	26621
Independent reflections	6805
Reflections with $I > 2\sigma(I)$	6031
R_{int}	0.0214
No. of parameters refined	510
GOF on F^2	1.088
$R_1{}^a/wR_2{}^b$ $(I > 2\sigma(I))$	0.0415/0.1150
$R_1{}^a/wR_2{}^b$ (all data)	0.0490/0.1285
Largest diff. peak and hole (e Å^{-3})	0.896 and -0.793

$^aR_1 = \Sigma||Fo| - |Fc||/\Sigma|Fo|$. $^bwR_2 = [\Sigma w(F_o^2 - F_c^2)^2/\Sigma w(F_o^2)^2]^{1/2}$, where $w = 1/[\sigma^2(F_o^2)+(aP)^2 + bP]$, $P = (F_o^2 + 2F_c^2)/3$.

SECTION S4

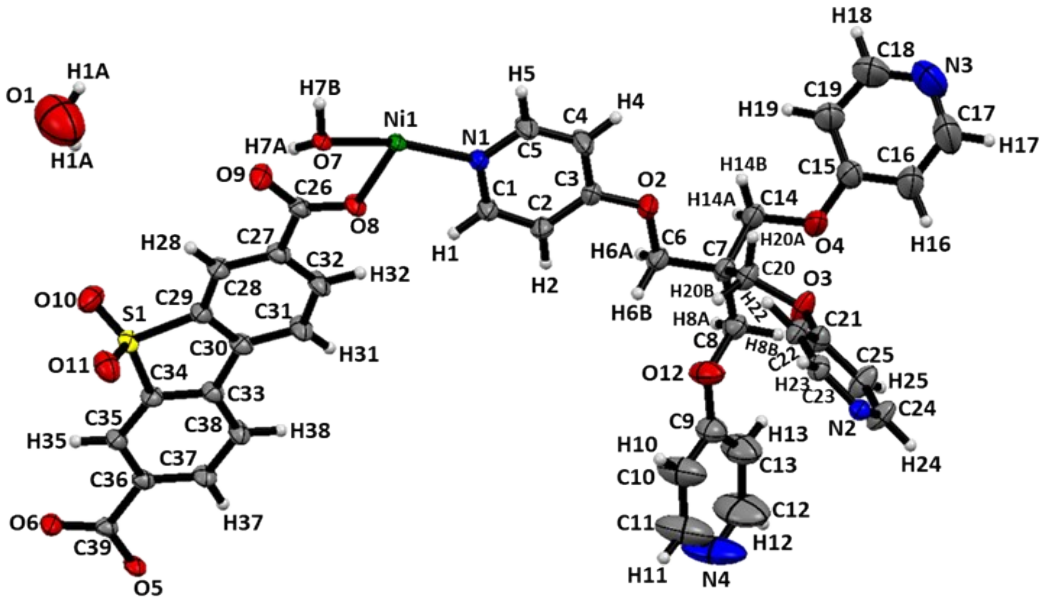

Fig. S1 ORTEP diagram of the asymmetric unit in **Ni-MOF** where nonhydrogen atoms are represented with ellipsoids at the 50% probability level.

SECTION S5

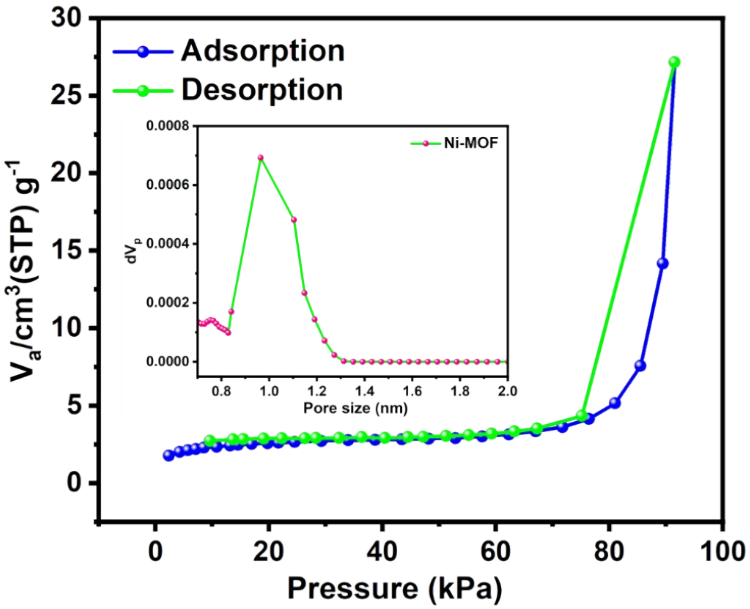

Fig. S2 Nitrogen sorption isotherm at 77 K (inset showing pore size analysis using the GCMC method).

SECTION S6

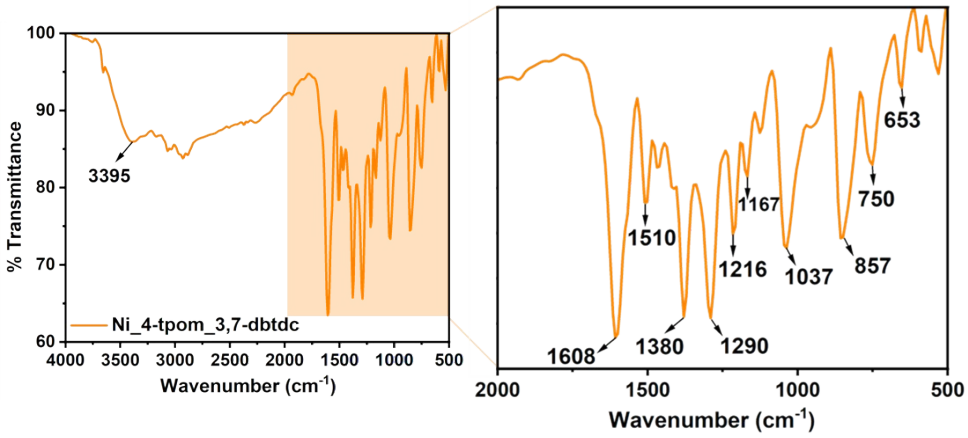

Fig. S3 FTIR spectra of as-synthesized **Ni-MOF**.

SECTION S7

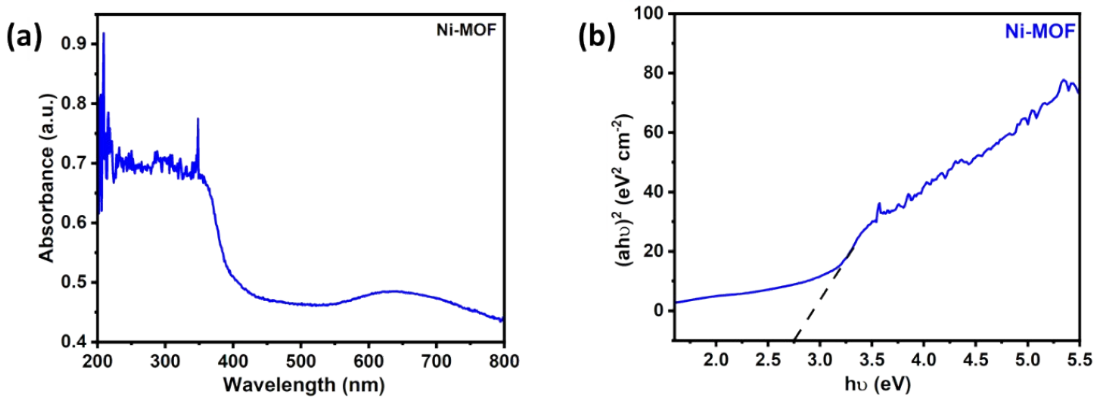

Fig. S4 (a) DRS and (b) Tauc plot of as-synthesized **Ni-MOF**.

SECTION S8

^{1}H NMR spectra of the crude product

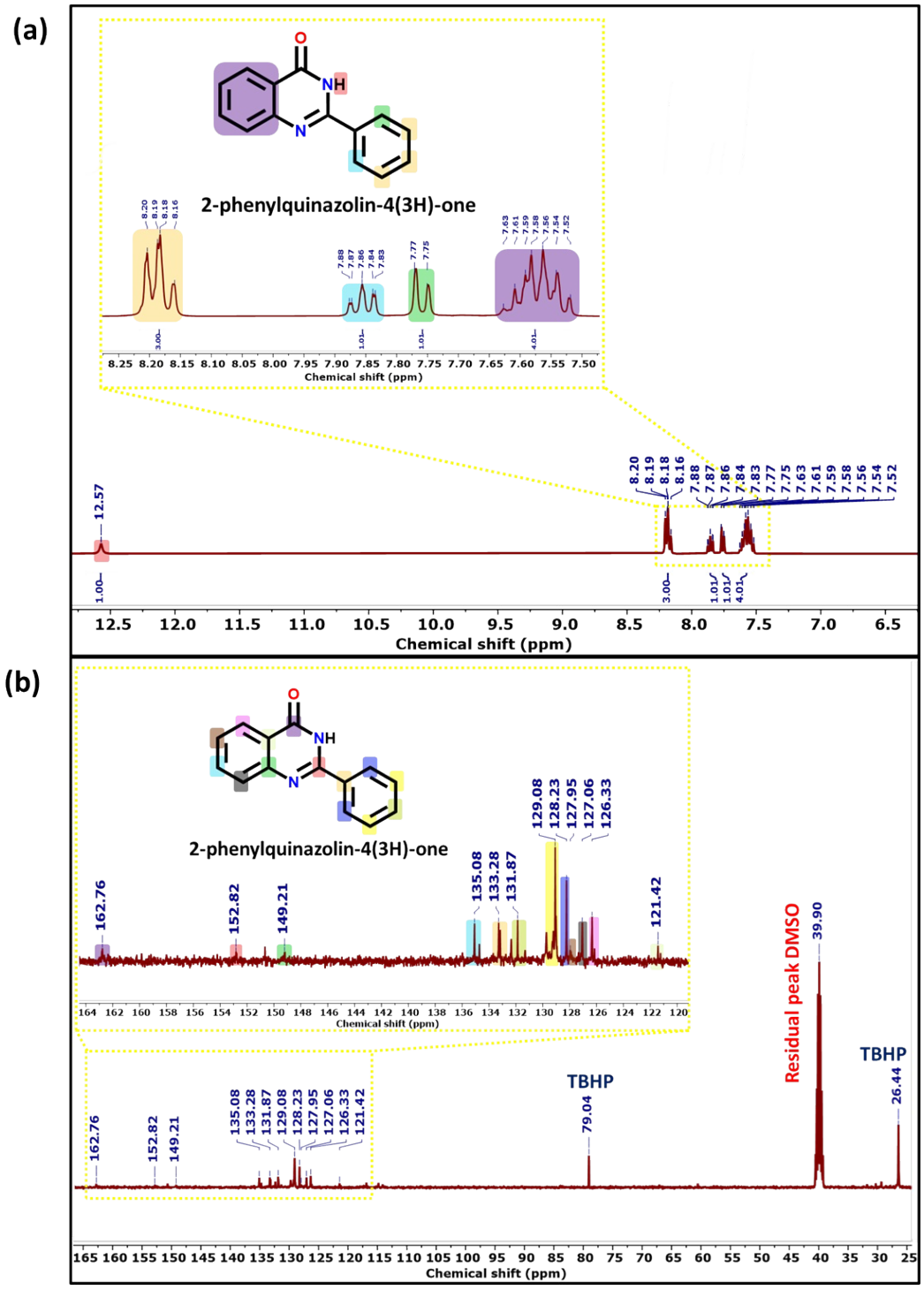

Fig. S5 (a) ^{1}H and (b) ^{13}C NMR spectra of the product (in DMSO-d6) for the entry 4 in Table 1, where 1 mol% **Ni-MOF** and 50 µL TBHP (70% in water) was used.

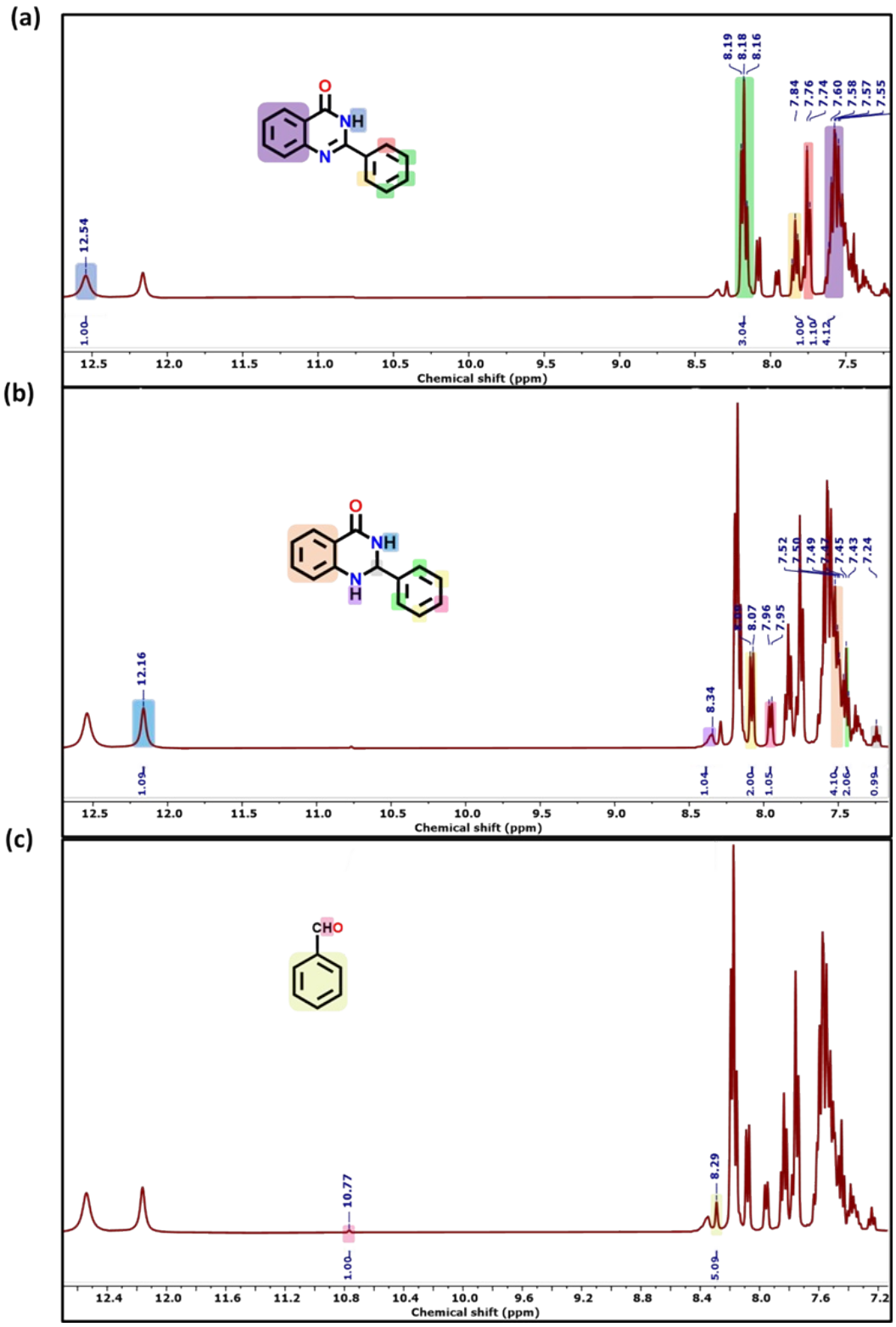

Fig. S6 [1]H NMR spectra of the crude product (in DMSO-d6) displaying signals for the (a) product, (b) intermediate B and (c) reactant for the entry 8 in Table 1, where 2 mol % **Ni-MOF** and 50 µL TBHP (70% in water) was used.

SECTION S9

^{1}H NMR spectra for the substrate diversity in benzaldehyde

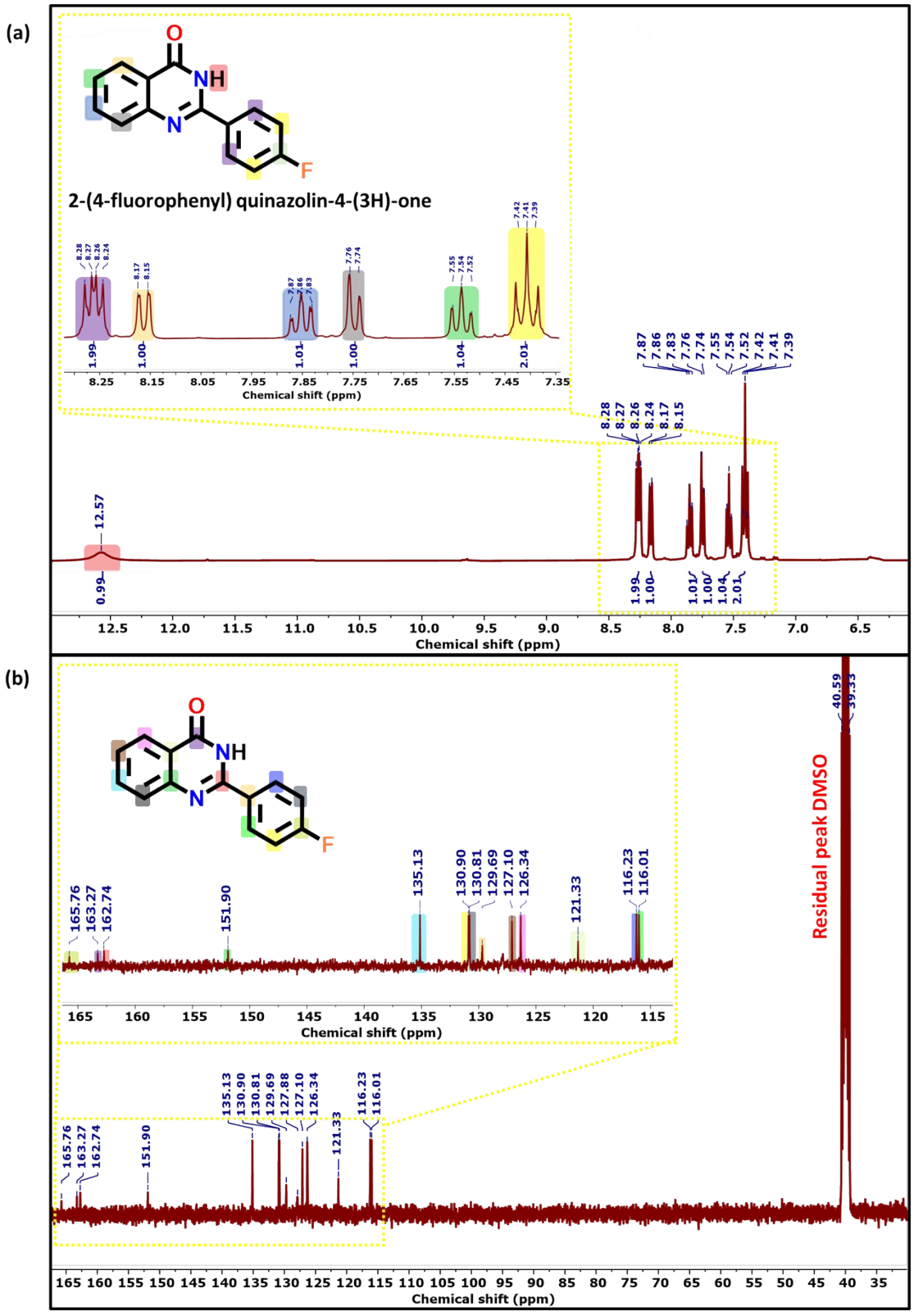

Fig. S7 (a) ^{1}H and (b) ^{13}C NMR spectra of the isolated product (in DMSO-d6) for the entry 1 in Table 2, where 2 mol% **Ni-MOF** and 50 µL TBHP (70% in water) was used.

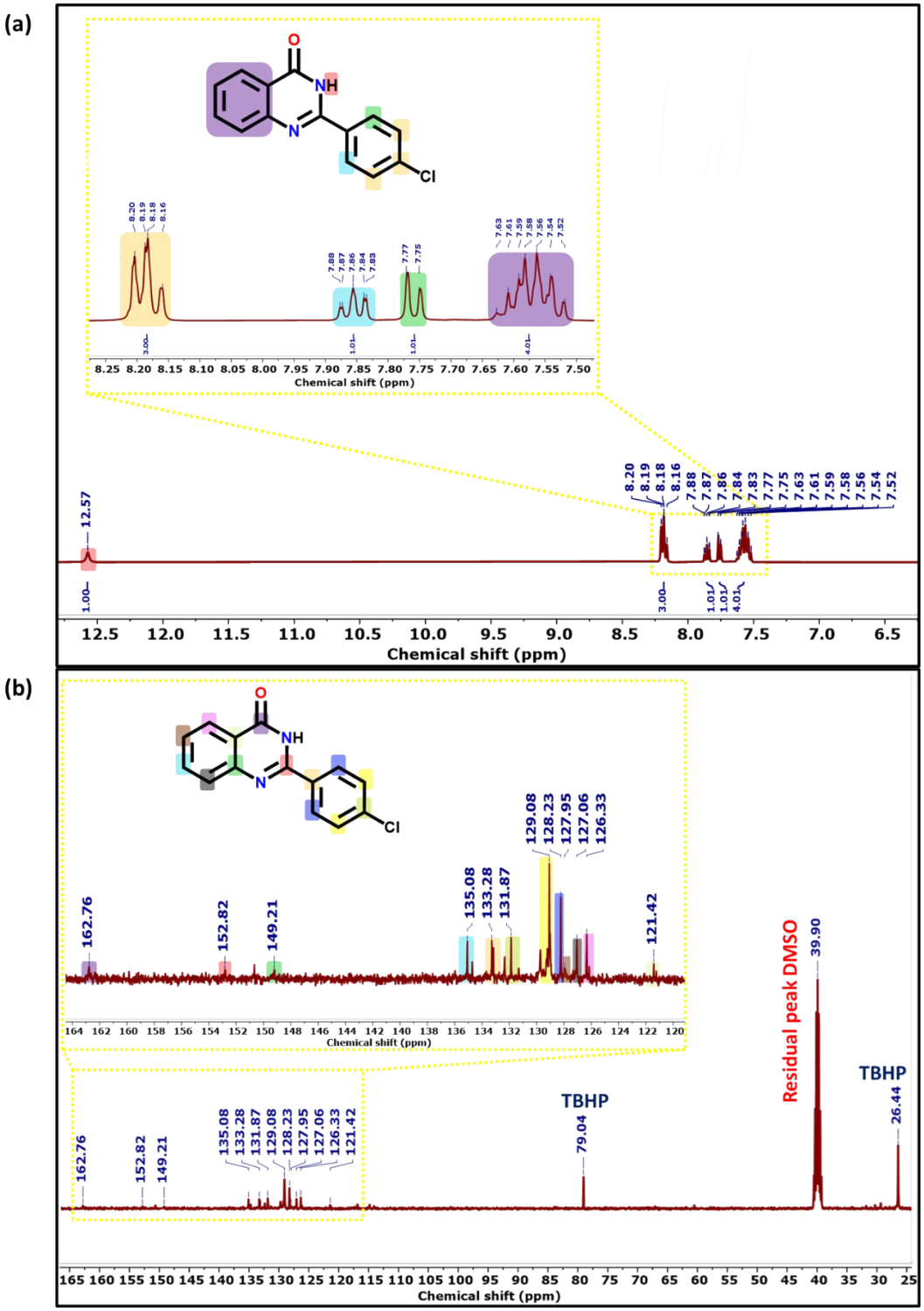

Fig. S8 (a) ^{1}H and (b) ^{13}C NMR spectra of the isolated product (in DMSO-d6) for the entry 2 in Table 2, where 2 mol% **Ni-MOF** and 50 µL TBHP (70% in water) was used.

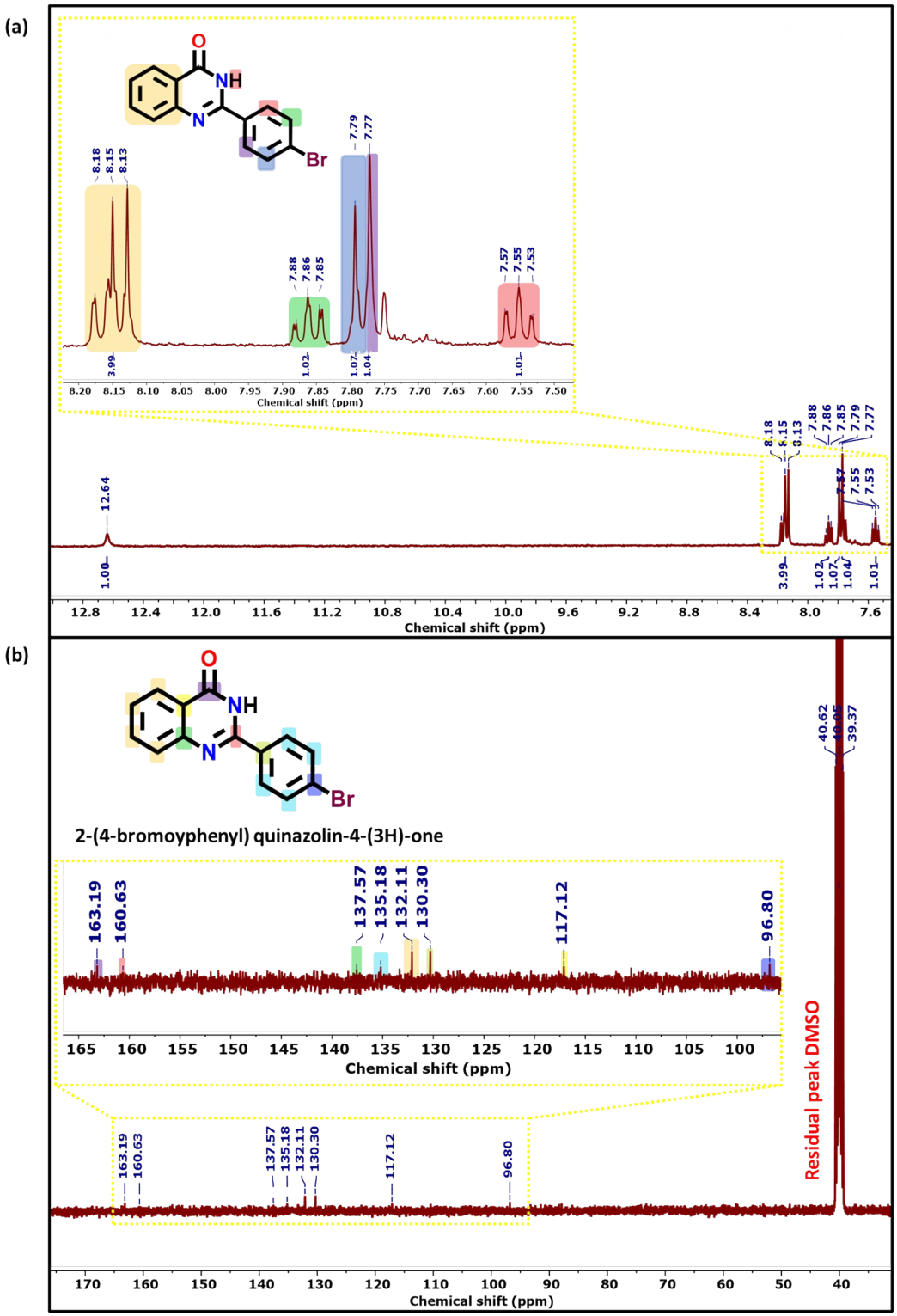

Fig. S9 (a) ^{1}H and (b) ^{13}C NMR spectra of the isolated product (in DMSO-d6) for the entry 3 in Table 2, where 2 mol% **Ni-MOF** and 50 µL TBHP (70% in water) was used.

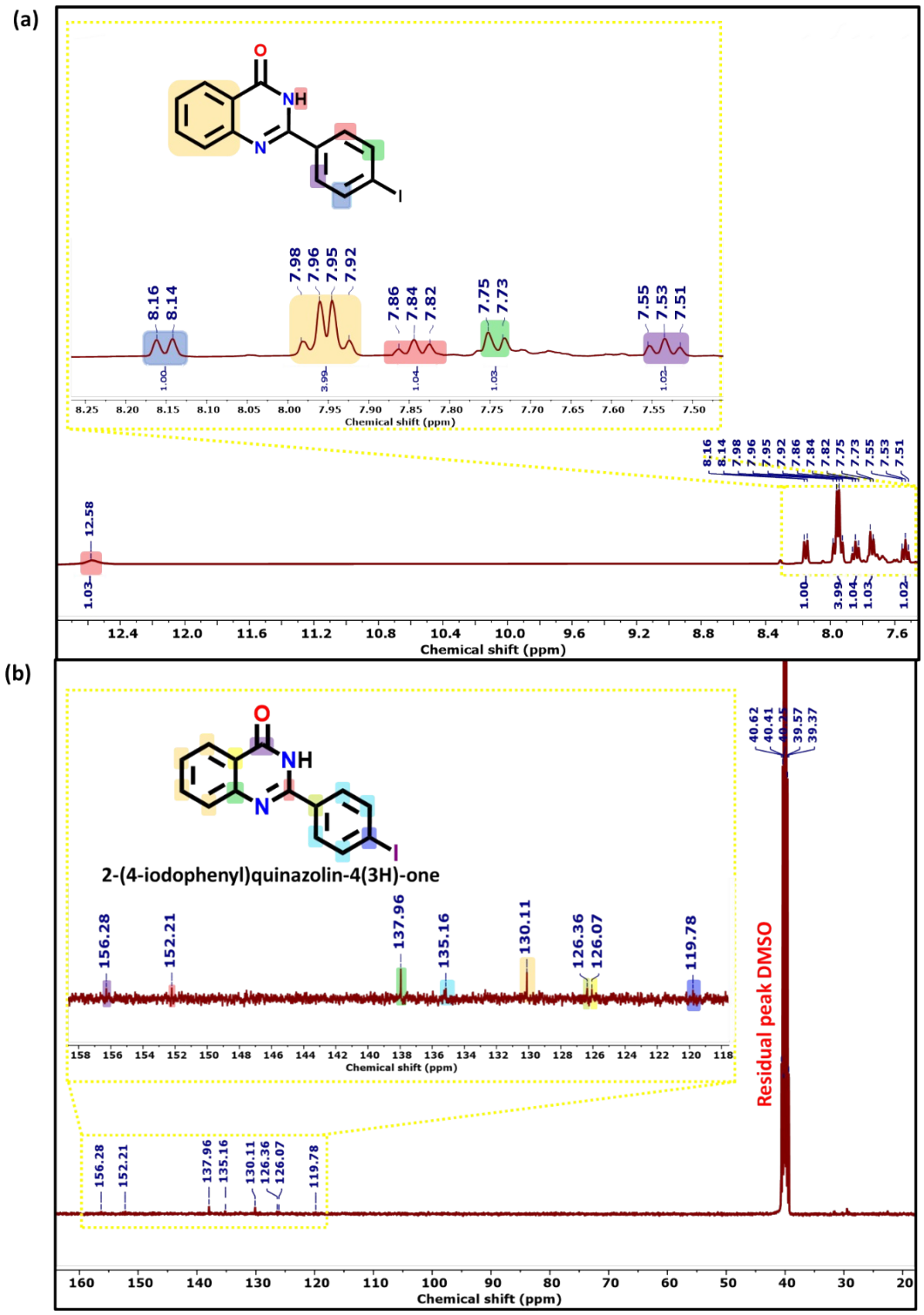

Fig. S10 (a) ^{1}H and (b) ^{13}C NMR spectra of the isolated product (in DMSO-d6) for the entry 4 in Table 2, where 2 mol% **Ni-MOF** and 50 µL TBHP (70% in water) was used.

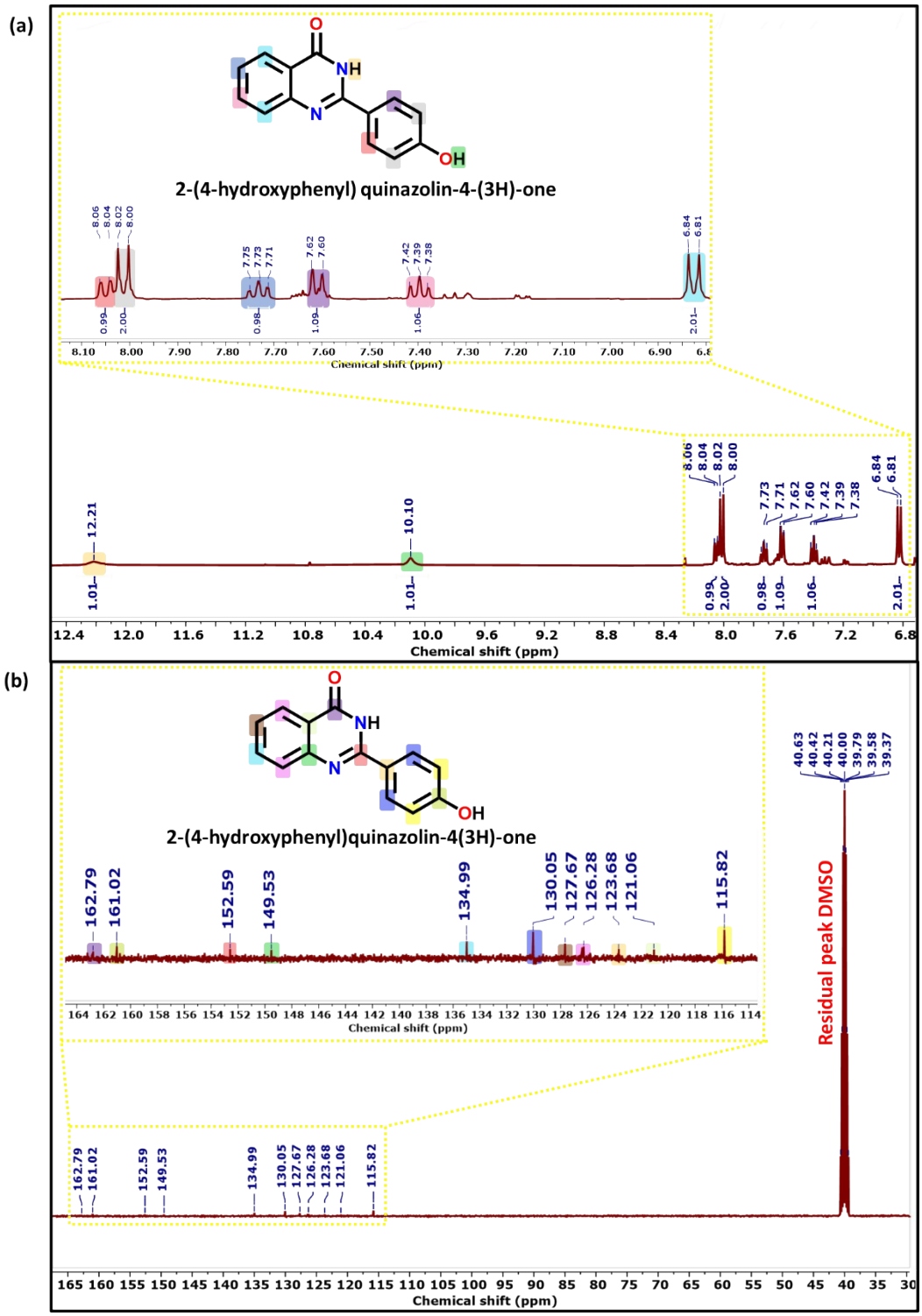

Fig. S11 (a) ^{1}H and (b) ^{13}C NMR spectra of the isolated product (in DMSO-d6) for the entry 5 in Table 2, where 2 mol% **Ni-MOF** and 50 µL TBHP (70% in water) was used.

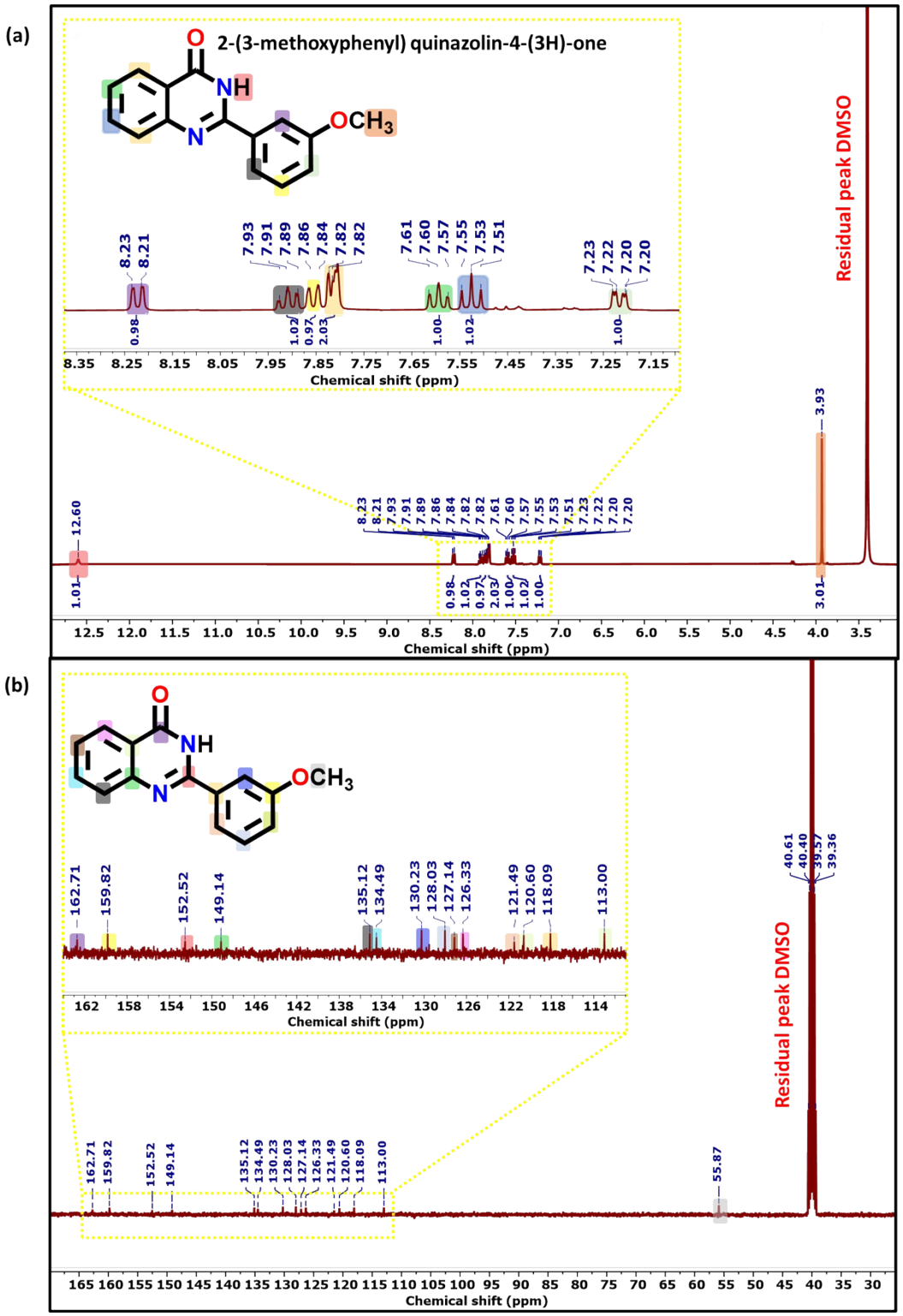

Fig. S12 (a) ^{1}H and (b) ^{13}C NMR spectra of the isolated product (in DMSO-d6) for the entry 6 in Table 2, where 2 mol% **Ni-MOF** and 50 µL TBHP (70% in water) was used.

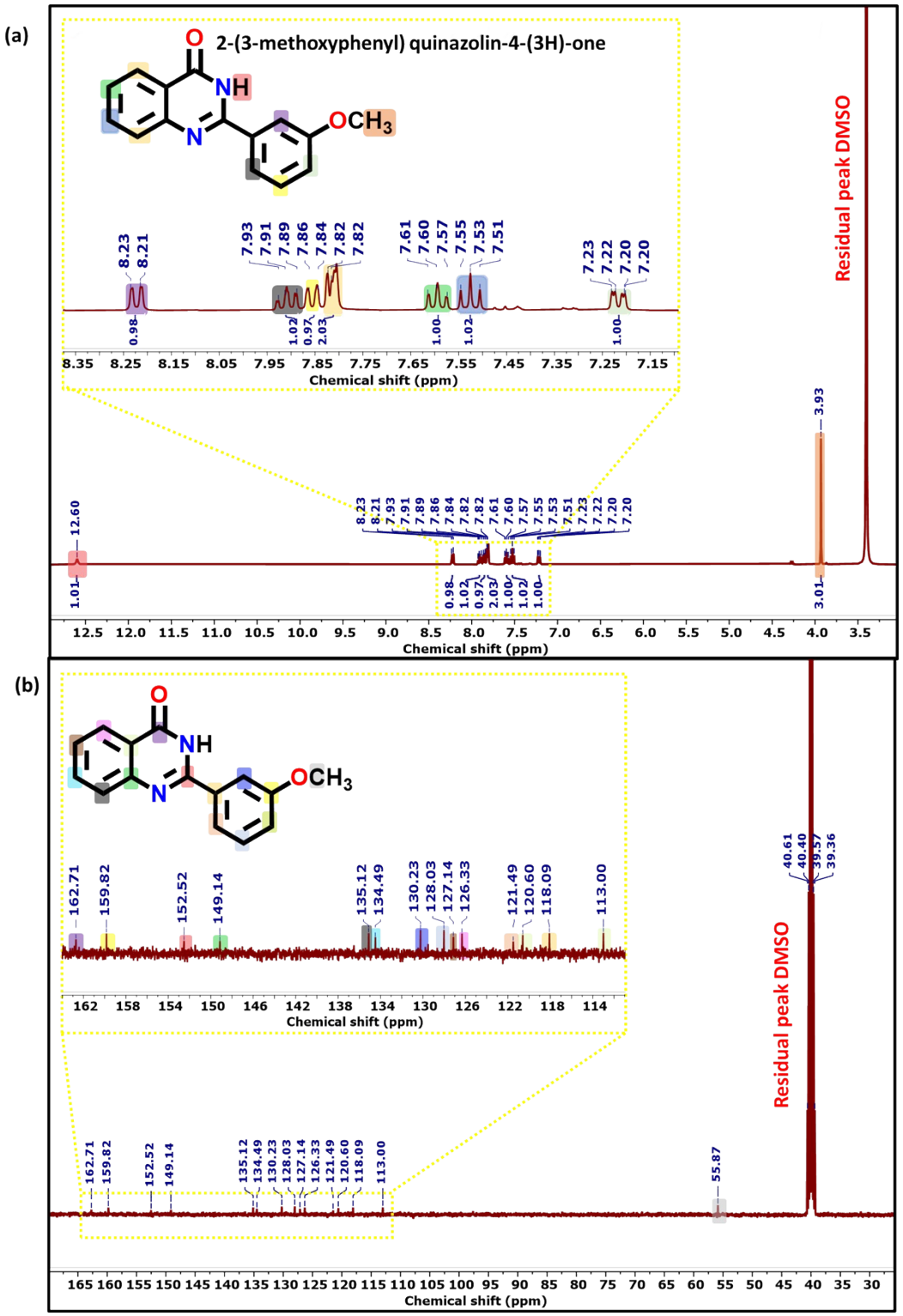

Fig. S13 (a) ^{1}H and (b) ^{13}C NMR spectra of the isolated product (in DMSO-d6) for the entry 7 in Table 2, where 2 mol% **Ni-MOF** and 50 µL TBHP (70% in water) was used.

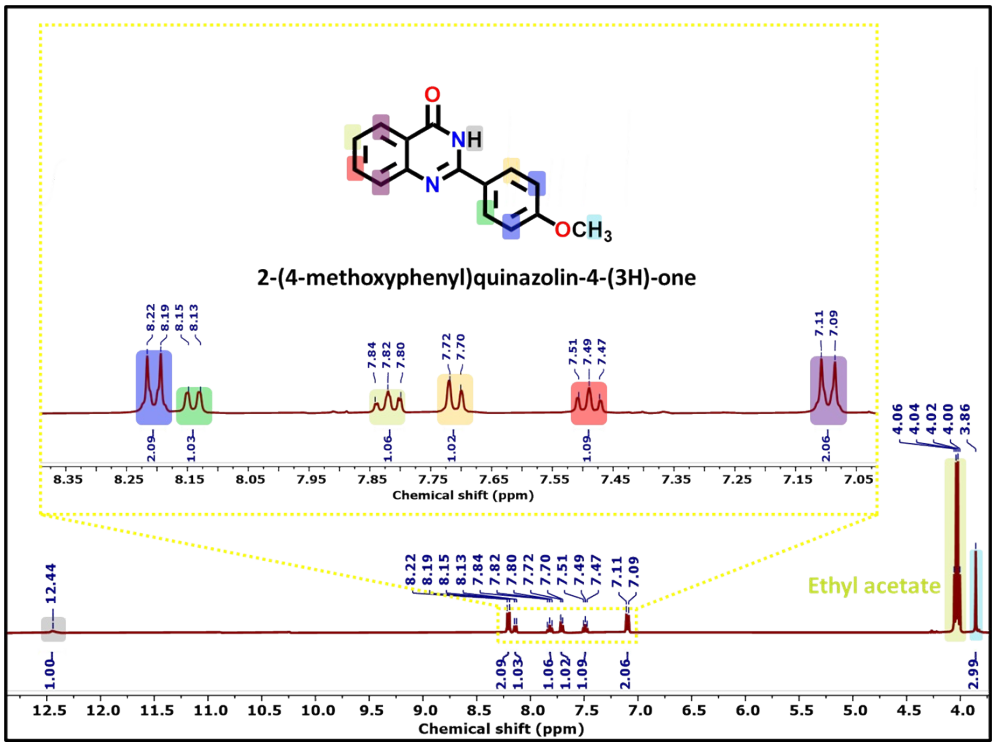

Fig. S14 (a) ^{1}H NMR spectra of the isolated product (in DMSO-d6) for the entry 8 in Table 2, where 2 mol% **Ni-MOF** and 50 µL TBHP (70% in water) was used.

SECTION S10

Table S2. Comparison of catalytic performance of **Ni-MOF** with relevant catalysts used for the synthesis of quinazolinones.

Sr. No.	Catalytic system	Catalyst amount	Oxidant (amount)	Temp. (°C)/Light source	Time (h)	Solvent	Yield	Reference
1.	**Ni-MOF**	**2 mol%**	**TBHP (70% in H_2O) (50 µL)**	**90**	**6**	**H_2O:THF (4:1, v/v)**	**99.9**	**This work**
2.	$[Cu^{I}4(4,4'\text{-bipy})_7(H_2PMo_9V_3O_{40})]\cdot 2H_2O$	1.2 mmol%	O_2	90	1	Dichloro ethane (DCE)	99	*ACS Appl. Mater. Interfaces*, 2024, **16**, 49400–49410
3.	SDUT-21	10 mg	TBHP (5.5 mol L^{-1})	80	12	DCE	99	*Inorg. Chem.*, 2023, **62**, 5565−5575
4.	SDUT-22	10 mg	TBHP (5.5 mol L^{-1})	80	12	DCE	53	*Inorg. Chem.*, 2023, **62**, 5565−5575
5.	Cu_2O nanoparticles	20 mol%	NaN_3[a]	80	26	PEG-400	92	*Green Chem.*, 2024, **26**, 4723–4732
6.	Fe-Fe_3C@NC-800	4 mol%	30% H_2O_2 in H_2O (0.4 mmol)	100	12	H_2O:THF (4:1)	91	*Chem. Sci.*, 2019, **10**, 10283–10289
7.	Zn(II) stabilized amidyl radical	5 mol%	LiO^tBu[b]	120	24		86	*Chem. Commun.*, 2024, **60**, 7097-7100
8.	Mn-based heterocycle	5 mol%	NaO^tBu[b]	140	36	Xylene	76	*Catal. Sci. Technol.*, 2022, **12**, 3202-3208
9.	Supramolecular assembly of Qx-Ind	1 mol%	air	12 W white LED	36	H_2O:DMSO (9:1)	88	*ACS Appl. Mater. Interfaces*, 2024, **16**, 67683–67696

[a]used as a reactant; [b]a base is used.

SECTION S11

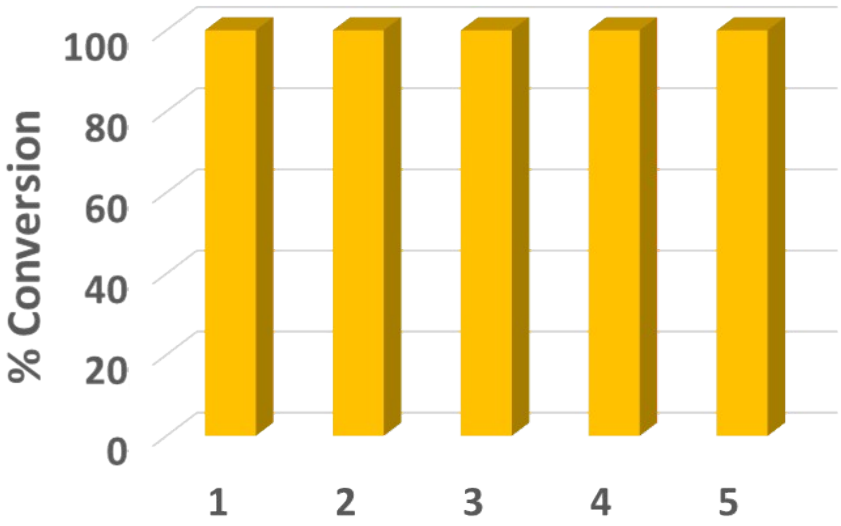

Fig. S15 Bar graph showing percentage conversion versus number of catalytic cycles showing the recyclability of **Ni-MOF** catalyst for the synthesis of quinazolinones from 2-aminobenzamide and benzaldehyde.

SECTION S12

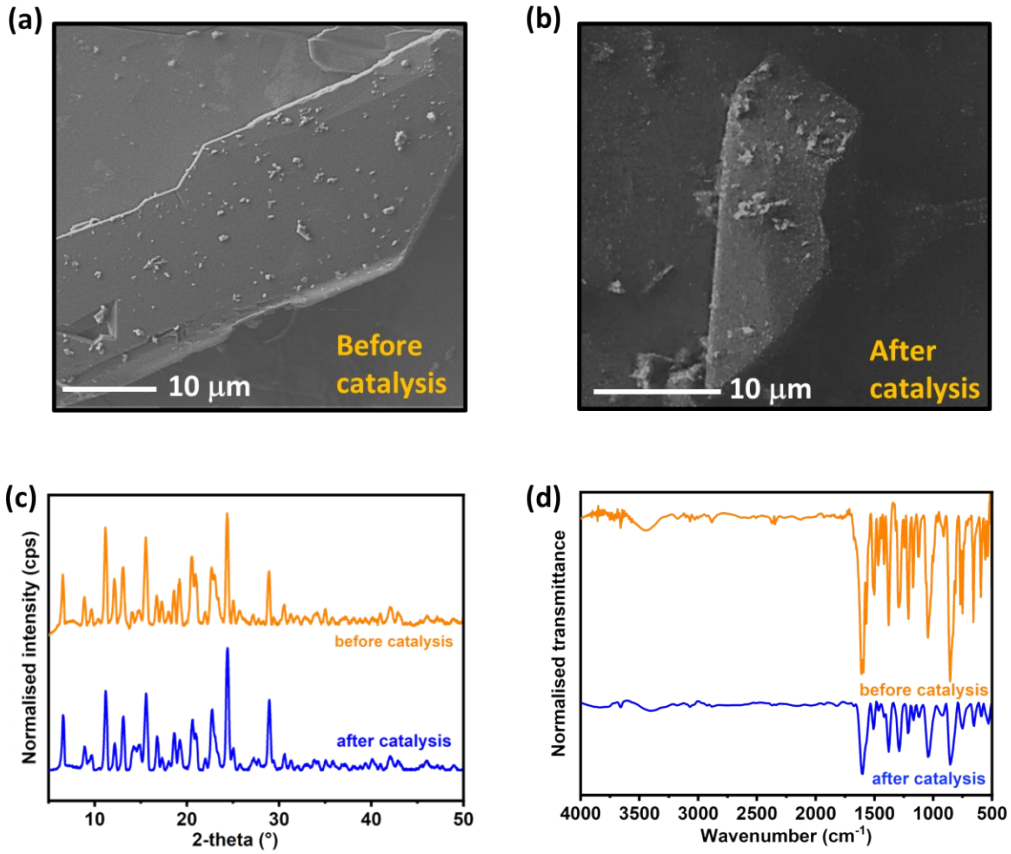

Fig. S16 Characterization of **Ni-MOF** before and after catalysis: (a,b) FESEM data, (c) powder X-ray diffractograms, and (d) FTIR spectra.

SECTION S13

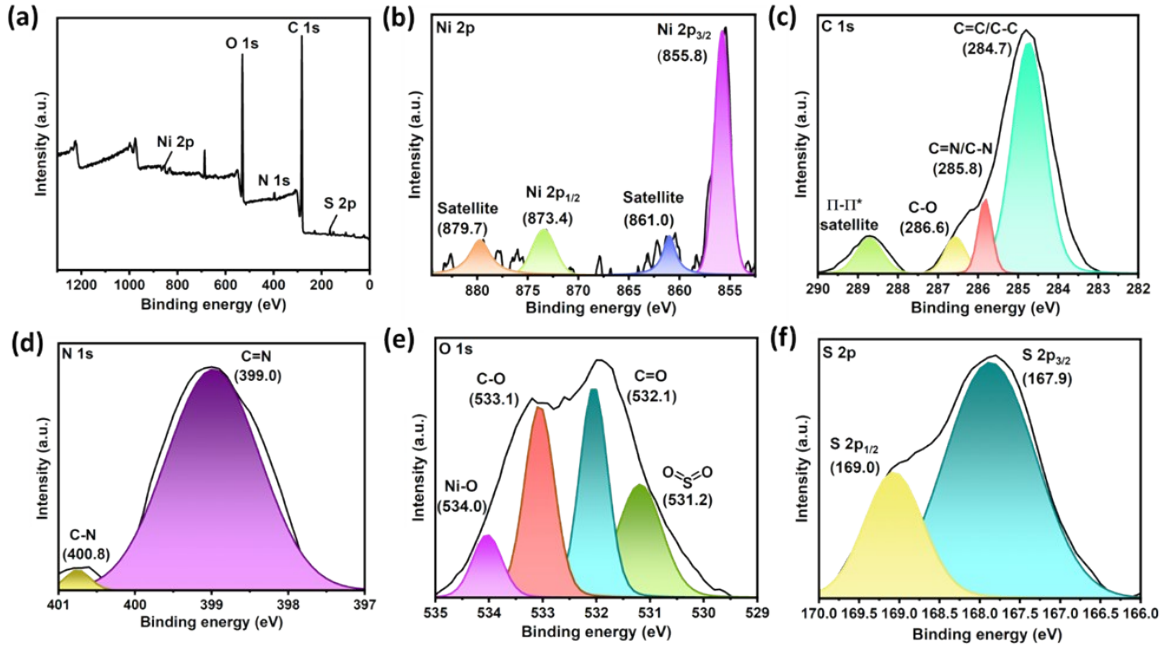

Fig. S17 X-ray photoelectron spectrum displaying (a) the full overlay and Deconvoluted XPS spectra of individual elements (b) Ni 2p, (c) C 1s, (d) N 1s, (e) O 1s and (f) S 2p of **Ni-MOF** after catalysis.

SECTION S14

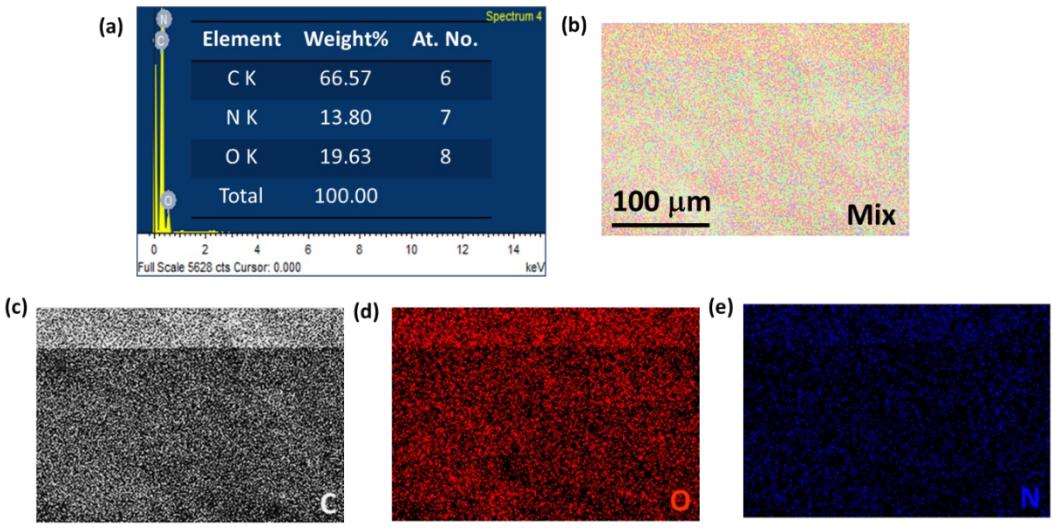

Fig. S18 (a) EDX examination and (b-e) Elemental mapping of the post-catalysis filtrate separation done by centrifugation and filtration followed by solvent evaporation.

SECTION S15

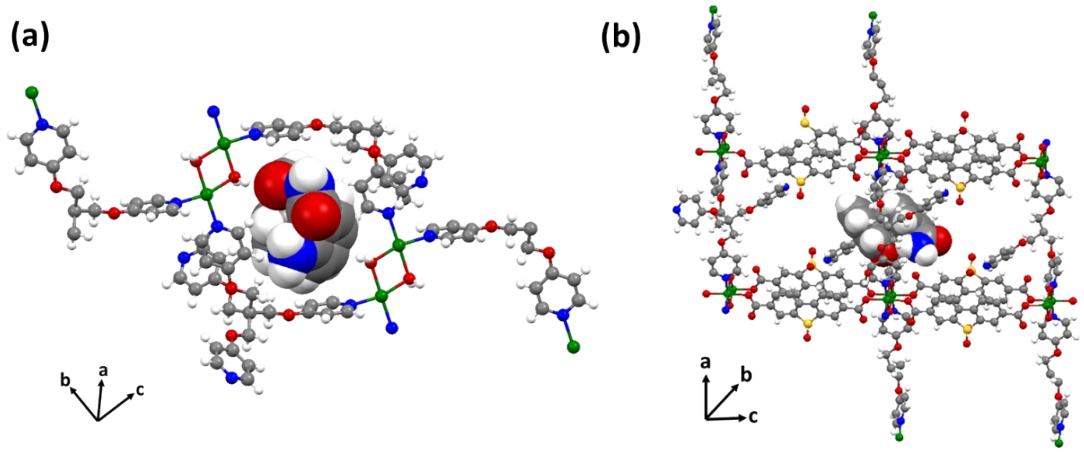

Fig. S19 Perspective views of the Ni-MOF structure along (a) the bc plane and (b) the ac plane, illustrating the encapsulation of benzaldehyde and 2-aminobenzamide within the pocket.

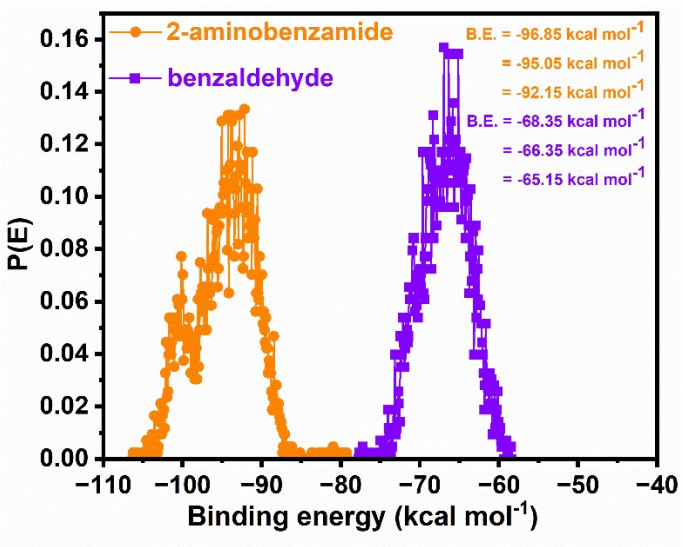

Fig. S20 Line profile showing binding energies of **Ni-MOF** after interaction with benzaldehyde and 2-aminobenzamide.

Model compounds for simulations

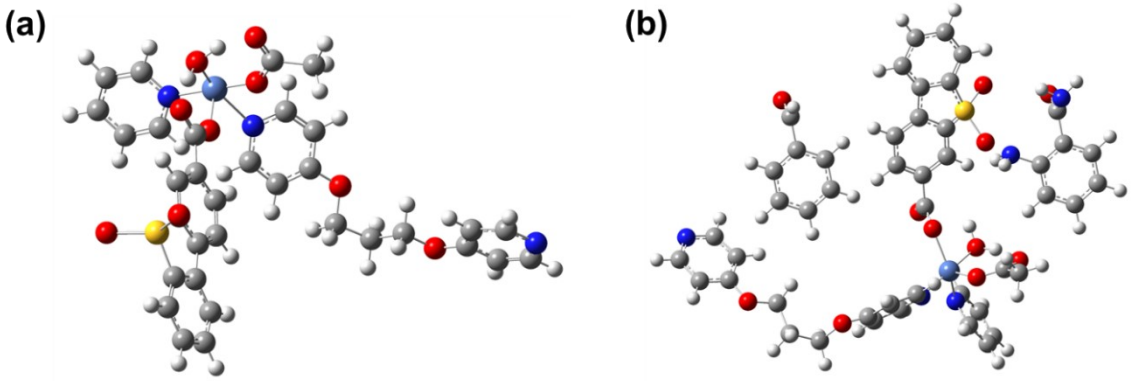

Fig. S21 Model compound replicating the **Ni-MOF** coordination environment: (a) **Ni-O** fragment; (b) optimized positioning of reactant molecules (2-aminobenzamide and benzaldehyde) near the **Ni-MOF** site via DFT simulations namely **Ni-R**.

Table S3. Optimized **Ni-R** Bond Critical Point (BCP) parameters from QTAIM analysis.

Bond Critical Point (BCP)	Distance (Å)	$\nabla^2\rho(r)$ Laplacian of electron density	G(r) Lagrangian kinetic energy	V(r) Potential energy density	H(r) Total energy density	-G(r)/V(r)
165 32(O)---88(H)	2.855	0.193580970 2E-01	0.365457107 8E-02	-0.246961790 0E-02	0.118495317 8E-02	1.48
175 15(H)---100(H)	2.548	0.110227952 3E-01	0.203580977 9E-02	-0.131592075 1E-02	0.719889028 5E-03	1.55
197 19(C)---99(H)	2.462	0.367558373 3E-01	0.788202443 9E-02	-0.657508954 6E-02	0.130693489 3E-02	1.20
199 108(N)---69(H)	2.011	0.11542900 28	0.289885542 0E-01	-0.291198576 9E-01	0.131303495 1E-03	1.00
238 107(H)---74(O)	2.831	0.218937817 6E-01	0.451626143 7E-02	-0.355907743 6E-02	0.9571840014 E-03	1.27
239 90(O)---74(O)	3.373	0.195126520 1E-01	0.416288244 1E-02	-0.344760188 0E-02	0.715280561 0E-03	1.21

SECTION S16

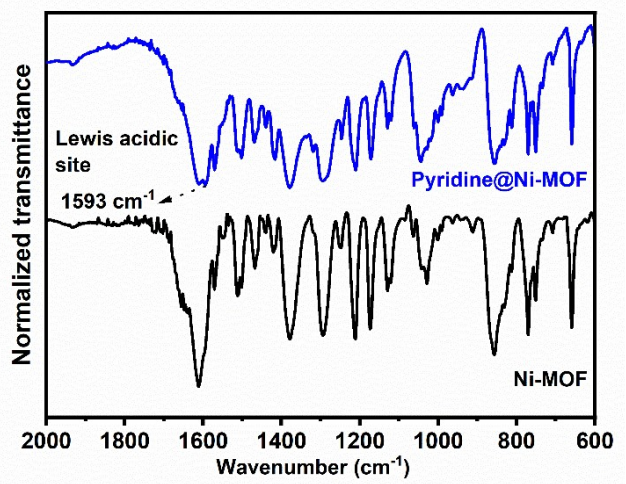

Fig. S22 FTIR spectra of **Ni-MOF** and pyridine treated **Ni-MOF**.

SECTION S17

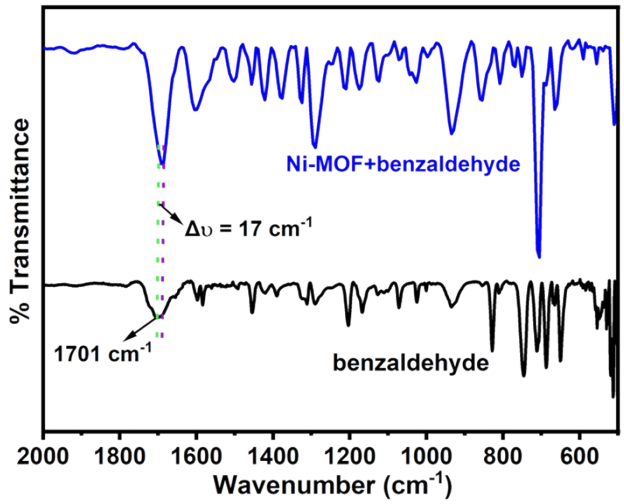

Fig. S23 Spectroscopic Evidence of interaction between benzaldehyde and **Ni-MOF**.

SECTION S18

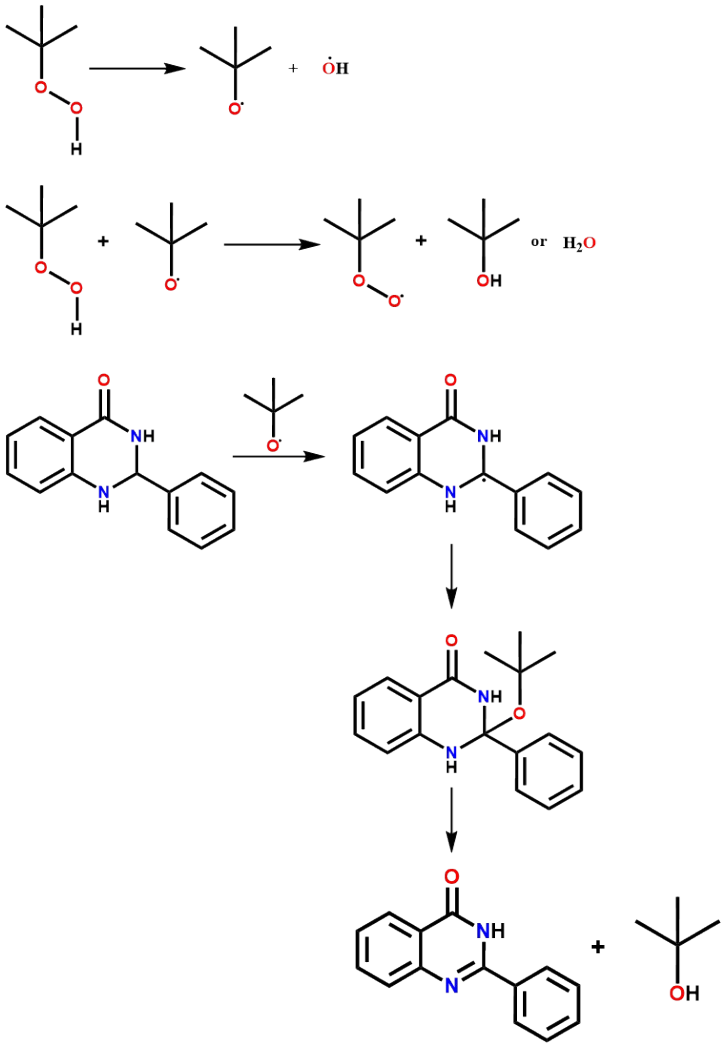

Fig. S24 Proposed radical mechanism for Dihydroquinazolinone to Quinazolinone Conversion and the adduct formation in presence of TEMPO.

SECTION S19

References

(S1) APEX2, SADABS, and SAINT; Bruker AXS Inc., Madison, WI, USA, 2008.

(S2) O. V. Dolomanov, L. J. Bourhis, R. J. Gildea, J. A. K. Howard, H. Puschmann, H. J. *Appl. Crystallogr.,* 2009, **42**, 339–341.

(S3) C. F. Macrae, I. J. Bruno, J. A. Chrisholm, P. R. Edgington, P. McCabe, L. Monge, R. Tayor, J. van de Streek, P. A. Wood. *J. Appl. Crystallogr.,* 2008, **41**, 466-470.

(S4) V. A. Blatov, A. P. Shevchenko, D.M. Proserpio. *Cryst. Growth Des.*, 2014, **14**, 3576–3586.

(S5) Dassault Systèmes BIOVIA, ViewerLite 5.0, San Diego: Dassault Systèmes, 2002.

(S6) M. J. Frisch, G. W. Trucks, H. B. Schlegal, G. E. Scuseria, M. A. Robb, J. R. Cheeseman, G. Scalmani, V. Barone, B. Mennucci, G. A. Petersson, H. Nakatsuji, M. Caricato, X. Li, H. P. Hratchian, A. F. Izmaylov, J. Bloino, G. Zheng, J. L. Sonnenberg, M. Hada, M. Ehara, K. Toyota, R. Fukuda, J. Hasegawa, M. Ishida, T. Nakajima, Y. Honda, O. Kitao, H. Nakai, T. Vreven, J. A. Montgomery, J. E. Peralta, F. Ogliaro, M. Bearpark, J. J. Heyd, E. Brothers, K. N. Kudin, V. N. Staroverov, R. Kobayashi, J. Normand, K. Raghavachari, A. Rendell, J. C. Burant, S. S. Iyengar, J. Tomasi, M. Cossi, N. Rega, J. M. Millam, M. Klene, J. E. Knox, J. B. Cross, V. Bakken, C. Adamo, J. Jaramillo, R. Gomperts, R. E. Stratmann, O. Yazyev, A. J. Austin, R. Cammi, C. Pomelli, J. W. Ochterski, R. L. Martin, K. Morokuma, V. G. Zakrzewski, G. A. Voth, P. Salvador, J. J. Dannenberg, S. Dapprich, A. D. Daniels, Ö. Farkas, J. B. Foresman, J. V. Ortiz, J. Cioslowski, D. J. Fox, Gaussian 09; Gaussian: Wallingford, CT, USA, 2013.

(S7) T. Lu, F. Chen. *J. Comput. Chem.*, 2012, **33**, 580-592.

(S8) W. Humphrey, A. Dalke, K. Schulten. *J. Molec. Graphics*, 1996, **14**, 33-38.